

Observations and temperatures of Io's Pele Patera from Cassini and Galileo spacecraft images

Jani Radebaugh,^{a,*} Alfred S. McEwen,^a Moses P. Milazzo,^a Laszlo P. Keszthelyi,^b
Ashley G. Davies,^c Elizabeth P. Turtle,^a and Douglas D. Dawson^a

^a Lunar and Planetary Laboratory, University of Arizona, Tucson, AZ 85721, USA

^b US Geological Survey, 2255 N. Gemini Dr., Flagstaff, AZ 86001, USA

^c Jet Propulsion Laboratory, 4800 Oak Grove Drive, Pasadena, CA 91109-8099, USA

Received 22 May 2003; revised 17 October 2003

Abstract

Pele has been the most intense high-temperature hotspot on Io to be continuously active during the Galileo monitoring from 1996–2001. A suite of characteristics suggests that Pele is an active lava lake inside a volcanic depression. In 2000–2001, Pele was observed by two spacecraft, Cassini and Galileo. The Cassini observations revealed that Pele is variable in activity over timescales of minutes, typical of active lava lakes in Hawaii and Ethiopia. These observations also revealed that the short-wavelength thermal emission from Pele decreases with rotation of Io by a factor significantly greater than the cosine of the emission angle, and that the color temperature becomes more variable and hotter at high emission angles. This behavior suggests that a significant portion of the visible thermal emission from Pele comes from lava fountains within a topographically confined lava body. High spatial resolution, nightside images from a Galileo flyby in October 2001 revealed a large, relatively cool (< 800 K) region, ringed by bright hotspots, and a central region of high thermal emission, which is hypothesized to be due to fountaining and convection in the lava lake. Images taken through different filters revealed color temperatures of 1500 ± 80 K from Cassini ISS data and 1605 ± 220 and 1420 ± 100 K from small portions of Galileo SSI data. Such temperatures are near the upper limit for basaltic compositions. Given the limitations of deriving lava eruption temperature in the absence of in situ measurement, it is possible that Pele has lavas with ultramafic compositions. The long-lived, vigorous activity of what is most likely an actively overturning lava lake in Pele Patera indicates that there is a strong connection to a large, stable magma source region.

© 2003 Elsevier Inc. All rights reserved.

Keywords: Satellites of Jupiter; Io; Volcanism; Surfaces-satellite; Interiors

1. Introduction and previous discoveries about Pele

Jupiter's moon Io lays claim to the hottest and most active volcanoes in the Solar System. Of the many volcanoes littering Io's surface, Pele Patera is one of the most distinctive and dramatic in its eruption style, activity level, and appearance (Smith et al., 1979; Spencer and Schneider, 1996; McEwen et al., 1998a). During the Voyager 1 flyby in 1979, Pele Patera was observed to be the source of a giant, 1200 km diameter, diffuse, red ring of deposits (Fig. 1), produced by a plume reaching 300 km in height (Strom et al., 1981). The plume was not observed by Voyager 2, but we now know from Galileo and Hubble Space Telescope (HST) ob-

servations that it may have been active but difficult to detect, like a "stealth" plume (Johnson et al., 1995). HST and Galileo observations suggest that the red material results from short-chain S, and that SO₂ is also present (Spencer et al., 1997a, 2000a, Geissler et al., 1999). The Solid State Imaging (SSI) camera on the Galileo spacecraft and HST have shown that the plume sometimes reaches ~ 450 km in height (Spencer et al., 1997a; McEwen et al., 1998a). Inward of the red deposits is a fan-shaped deposit of dark, diffuse material that extends to 150 km from its source and is likely to be composed of silicate pyroclastics ejected from Pele (Strom et al., 1979; Geissler et al., 1999).

Pele also exhibits continually high thermal emission. It was the hottest spot detected by Voyager, with a model temperature of 650 K (Pearl and Sinton, 1982) that suggested much hotter lava temperatures (Carr, 1986). Galileo observations made of Io during eclipse by Jupiter and of Io's

* Corresponding author.

E-mail address: jani@lpl.arizona.edu (J. Radebaugh).

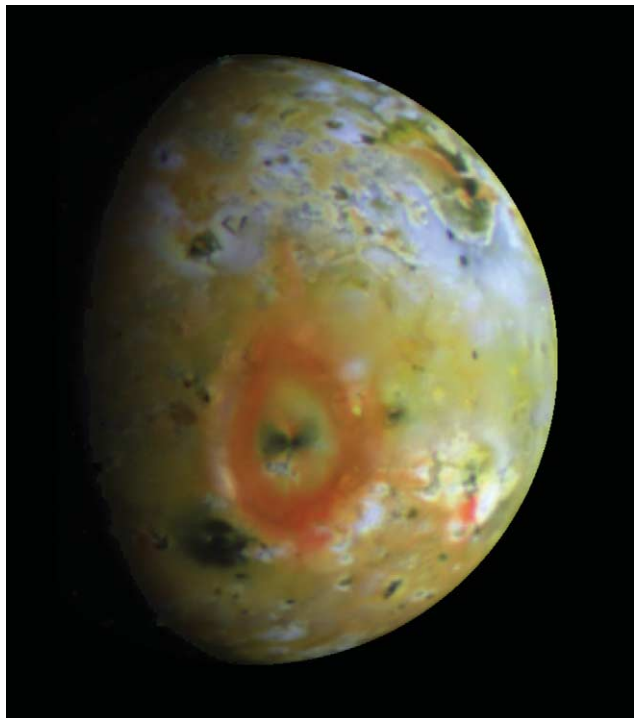


Fig. 1. Slightly enhanced color image of Io centered on 270° west longitude, taken by Galileo SSI during the G1 orbit, 27 June 1996. Pele Patera is surrounded by a fan of dark, pyroclastic material and a much larger, 1500 km diameter, red ring of sulfur-rich plume deposits. The color image is a combination of images taken through the near-IR, green, and violet filters and has a resolution of $\sim 14 \text{ km pixel}^{-1}$.

nightside revealed Pele to be a prominent hotspot throughout 1996–2001 (McEwen et al., 1998a; Keszthelyi et al., 2001). In many of these instances, the thermal output at Pele was so great that it saturated the SSI detector, preventing us from determining precise temperatures (Keszthelyi et al., 2001). Pele was also observed by Galileo's Photopolarimeter Radiometer (PPR) (Spencer et al., 2000b; Rathbun et al., 2004) and Near Infrared Mapping Spectrometer (NIMS) (Lopes-Gautier et al., 1999; Davies et al., 2001; Lopes et al., 2001, 2004), and by HST and ground-based telescopes (Spencer et al., 1997b; Marchis et al., 2001; in preparation). In fact, Pele has been active in every observation made during the Galileo era, although it may have been inactive for a period of time between Voyager and Galileo (Spencer and Schneider, 1996).

The tremendous thermal output observed at Pele is in contrast to the relatively small size of its patera (volcanotectonic depression), at least in comparison to other paterae on Io. Pele was best imaged in the daylight by Voyager 1, at about 1 km pixel^{-1} . It is an elongate depression, extending north from the plateau Danube Planum (Fig. 2) (Strom et al., 1979; McEwen et al., 2000). Its dimensions are $30 \text{ km} \times 20 \text{ km}$, less than the mean diameter for paterae on Io of 41 km and much smaller than the largest Ionian paterae, which are over 150 km in diameter (Radebaugh et al., 2001), but large compared with terrestrial basaltic calderas

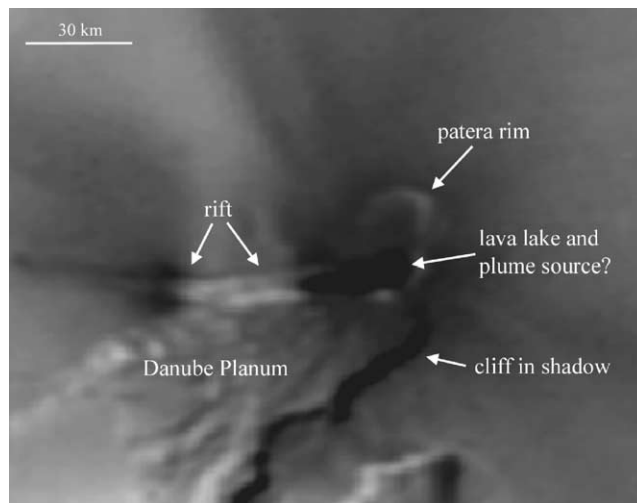


Fig. 2. The best resolution daytime image of Pele Patera is from Voyager in 1979. The Pele region is shown here at $\sim 2 \text{ km pixel}^{-1}$. The patera extends north from Danube Planum, a high plateau in the south center of this image. Pele Patera is also bounded on the south by a large, east-west trending rift. This rift shows evidence of current volcanic activity in the form of dark pyroclastic deposits bordering its west end, and dark material, likely lava flows, on its east end, in the south of the patera. The figure is taken from the USGS Flagstaff global Io Voyager basemap. North is toward the top of the image.

(mean 6.6 km; Radebaugh, 1999). The activity at Pele appears to be confined to the southern portion of this patera, since low-albedo materials associated with high-T hotspots on Io (McEwen et al., 1985, 1997) are found there. This region also coincides with a large rift that runs parallel to the north margin of Danube Planum and the south margin of Pele Patera (Fig. 2). NIMS observed high thermal output at the southeast corner of Pele Patera during orbit I27, in February 2000 (Lopes et al., 2001; Davies et al., 2001). Lower resolution ($\geq 3 \text{ km pixel}^{-1}$) visible images from Galileo show that there are no large lava flows currently emerging from Pele Patera. However, NIMS spectra of thermal emission show persistent, elevated thermal emission peaking at wavelengths shorter than $3 \mu\text{m}$, indicating a vigorous eruption that is constantly exposing new lava. These data were interpreted by Davies et al. (2001) as due to an active lava lake with a crust disrupted by lava fountaining, which reinforced a similar conclusion by Howell (1997) from groundbased data. A lava lake is defined as a volcanic depression that contains exposed liquid lava, overlying and directly connected to a magma source. This feature reveals, through energy output, the mass flux which in turn can be used to determine the interior plumbing of the volcano (Harris et al., 1999; Davies, 2003).

During the Galileo I24 flyby of Io, SSI obtained nightside observations of Pele Patera at 30 m pixel^{-1} . Only a curving line of glowing spots, more than 10 km long and 50 m wide (Fig. 3) was observed. It was suggested that the line of hotspots marked the edge of Pele Patera (which may also coincide with a margin of the rift) and that the chilled crust of a

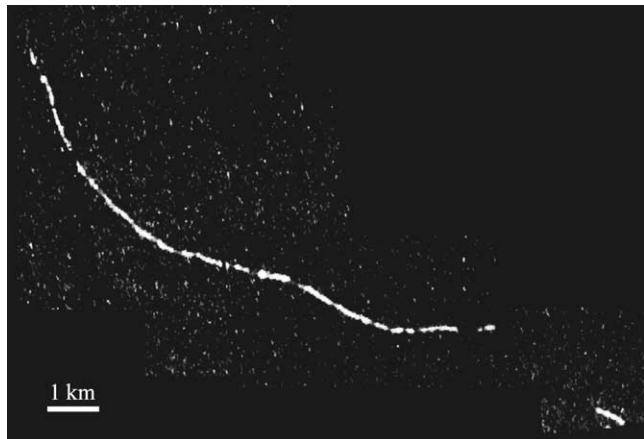


Fig. 3. A bright, curving line of hotspots is seen here in nightside images of the Pele region from the Galileo I24 orbit, 11 October 1999. This image was taken through SSI's clear filter. The bright regions resemble the margins of terrestrial lava lakes where the chilled crust breaks up against the confining walls, exposing the hot lava beneath. Image resolution is $\sim 30 \text{ m pixel}^{-1}$, north is toward the top.

lava lake was breaking up against the patera walls, exposing the underlying, hot, liquid lava (McEwen et al., 2000).

Previously published Galileo-derived temperature estimates included $1275 \pm 15 \text{ K}$ from an SSI eclipse observation in 1997 (McEwen et al., 1998b). In addition, Lopes et al. (2001) reported a median temperature of $1760 \text{ K} (\pm 210 \text{ K})$ for the high temperature component of fits to 15 hand-picked pixels within the largely-saturated, high-spatial resolution I24 NIMS data. Maximum surface temperatures derived from a fit to a combined NIMS-SSI dataset using a model of volcanic thermal emission (Davies, 1996) yielded a liquidus range of $1250\text{--}1475 \text{ K}$. Davies et al. (2001) found that the high-temperature components of two-temperature fits to NIMS data ranged from 1077 ± 13 to $1390 \pm 25 \text{ K}$, but concluded that the magma temperature needed to be $> 1600 \text{ K}$ to explain this thermal signature.

2. New observations

The main objective of this paper is to present the latest spacecraft observations of Pele Patera. In this section, we describe these data and briefly explain how we derive lava temperatures. While most of the details of the data analysis are in the appendices, it is important to note that these temperatures could only be retrieved with such precision because of the exquisite calibration of the cameras on both Galileo and Cassini. Most of the techniques we use have not been applied to terrestrial remote sensing data from volcanoes on the Earth because such rigorous calibration data is not generally available. The discussion of how our new results have changed our understanding of the nature of the eruption occurring at Pele Patera is presented in later sections.

In late December 2000, the Cassini spacecraft passed near Jupiter, to gain a boost on its long journey to Saturn (Miner,



Fig. 4. Clear filter (CL1-CL2) image of Io by Cassini ISS, obtained 1 January 2001, while Io was in eclipse by Jupiter. The brightest hotspot south and east of center is Pele, the smaller one to the east of Pele is Pillan. Emissions near Io's limb are auroral glows from excitation of plume gases. Image resolution is $\sim 61 \text{ km pixel}^{-1}$.

2002). Cassini obtained four sets of multiple-filter images of Io in Jupiter's shadow, and Pele was the most prominent of the hotspots observed (Radebaugh and McEwen, 2001; Porco et al., 2003). Cassini's closest approach to Jupiter was 9.72 million kilometers, so it did not image Io with the high resolution of Voyager or Galileo. Still, at $\sim 61 \text{ km pixel}^{-1}$, the eclipse images revealed several bright hotspots, Pele being by far the most radiant (Fig. 4).

Ten months later, Galileo flew to within only 200 km of Io's surface, and obtained nightside images of Pele through two filters at 60 m pixel^{-1} (I32 flyby, October 2001; Turtle et al., 2004). These observations provided us with much-awaited details of the eruption morphology of the Pele volcanic center.

2.1. Cassini eclipse observations

Io passes through Jupiter's shadow every 42.5 hours. During Cassini's flyby of the jovian system, the narrow angle camera (NAC) of its Imaging Science Subsystem (ISS) returned close to 500 images of Io in eclipse (Porco et al., 2003). This suite of images was unique for Io because of its high temporal resolution, wavelength range, and radiometric precision. Imaging sequences lasted from two to three hours, with individual images separated from each other by just several seconds to minutes (Table 1). Clear filter observations were spaced ~ 11 minutes apart, the first time variability in Io's hotspot activity had been monitored from a spacecraft over such short time scales. The Cassini ISS camera provides 12 NAC filters resulting in 144 filter combinations to cover the wavelength range of $250\text{--}1050 \text{ nm}$, a major improvement over the 8 filters across $350\text{--}1100 \text{ nm}$ for Galileo's SSI. Furthermore, Cassini's ISS records data at $12\text{-bits pixel}^{-1}$ as opposed to Galileo SSI's 8-bits pixel^{-1} .

2.1.1. Color temperatures from Cassini eclipse images

We obtained two-filter ratio temperatures of the Pele hotspot from the Cassini eclipse data. Details of our method, including error analysis, are in Appendix A.1. The temperatures, for all three sets of eclipse observations, are between

Table 1
Details of the Cassini eclipse observations of Io

Eclipse observation	Start of imaging	End of imaging	SSC Lat	SSC Lon	Clear filter exp time	IR filter exp time	Time between clear and IR	Time between pairs
day364	2000 DEC 29, 09:07:44.51	2000 DEC 29, 12:07:44.51	~ 0.5° N	300°–324° W	0.046 s	0.197 s	48 s	11 min 12 s
day000	2000 DEC 31, 03:07:44.51	2000 DEC 31, 05:07:44.51	~ 0.2° S	286°–302° W	0.046 s	0.197 s	3 min 13 s	5 min 35 s
day001	2001 JAN 1, 22:07:44.51	2001 JAN 2, 01:07:44.51	~ 0.8° S	280°–305° W	0.046 s	0.197 s	48 s	11 min 12 s

Each observation is given a name corresponding to the day in the year 2000 or 2001. Data for the first planned eclipse observation, which would have been acquired during December 27, 2000, were not acquired due to a reaction wheel anomaly. Image times are recorded in hundredths of seconds. “SSC Lat” and “SSC Lon” indicate spacecraft latitude and longitude. “Time between clear” and “Time between IR” are the times between the consecutive clear and infrared images that were analyzed in pairs. This separation was much greater for day000 than for the other two eclipse observations, so interpretation of the ratios that result from this observation must be done with caution. “Time between pairs” is the time elapsed between consecutive clear filter images used for pair analysis. For this paper we analyzed ten image pairs for the day364 and day001 observations, and four image pairs for the day000 observation.

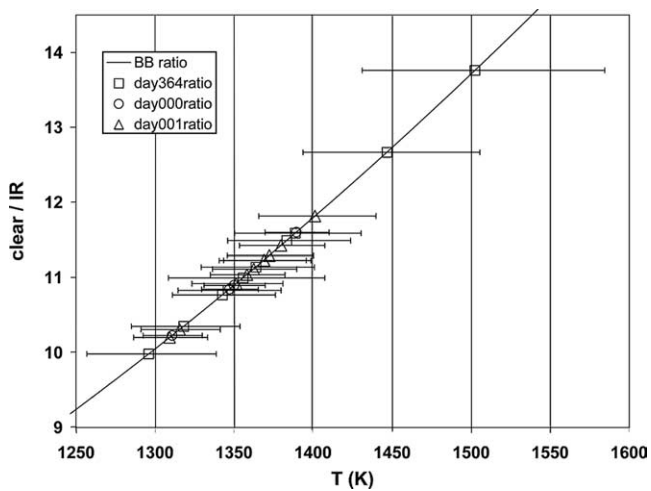


Fig. 5. Ratios of emission through Cassini’s clear and IR filters, plotted on the curve of ratios of expected blackbody emissions from Fig. A.1 (Appendix A.1), in order to determine color temperature. Plotted error bars are $> 1\sigma$. Most data points are clustered between 1350 and 1400 K.

1260 and 1580 K (including ~ 1 sigma error bars) as illustrated in Fig. 5. However, the temperatures are generally tightly clustered around a median value of 1360 K. These values are consistent with other temperatures estimated from Galileo observations of Pele, as discussed in Section 1.

2.1.2. Variation over time

Because Cassini obtained multiple image pairs over the course of each eclipse, we were able to observe changes in intensity and temperature at Pele over time. Overall intensity declined over the course of each eclipse observation. This is because as Pele rotated toward the east limb of Io the camera received less of the volcano’s overall emission (Fig. 6). If the volcano were a perfectly flat radiator, during each observation ISS should have seen a decrease in emission from Pele by a factor of the cosine of the emission angle. However, the observed emission from Pele requires a correction factor of $[\cos(\text{emission angle})]^{1.6}$ (Fig. 6). The interesting implications this may have for the geometry of the hot material within Pele is discussed later.

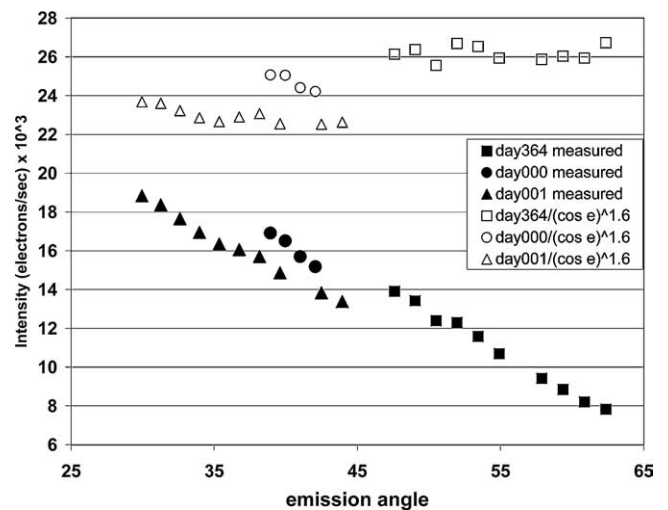


Fig. 6. Intensity in electrons s^{-1} for each eclipse observation, clear filter only. Open symbols are corrected for emission angle using $[\cos(\text{emission angle})]^{1.6}$ as described in the text. Uncorrected data (filled symbols) show a linear decrease in intensity with emission angle, although the day001 and day364/day000 data are offset, likely due to a decrease in emission from Pele in the later eclipse.

The temperatures from individual ratios are plotted against emission angle in Fig. 7. Since emission angle increased over time during each observation, this plot illustrates temperature changes at Pele over the course of each eclipse observation. All temperatures are fairly constant and are close to the median value of 1360 K. The exception is the last half of the first eclipse observation, day364 (December 29, 2000), which shows statistically significant oscillations in temperature from the lowest (1300 ± 40 K) to the highest value (1500 ± 80 K) within just 22 minutes. This temperature change also coincides with the highest emission angle of any of the observations. Temperatures for day000 (December 31, 2000) and day001 (January 1, 2001) also show minor variations. There is a slight downturn in temperature at the end of day000, and the second half of day001 shows a drop in temperature, followed by a steady increase. However, these are fairly minor variations compared with the dramatic oscillations from day364.

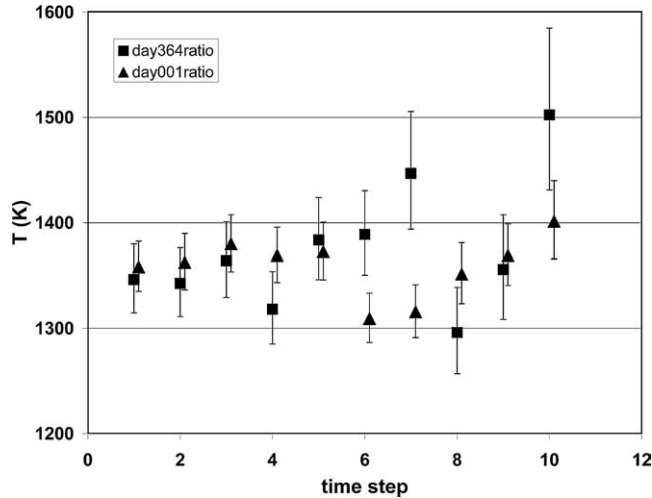


Fig. 7. Variation in temperature against clear filter emission angle is shown for all three eclipse observations. Each eclipse observation progresses in time from left to right. Temperatures result from ratios of CL1–CL2 to IR4–CL2 images. Values are generally equivalent to the mean value of 1360 K derived for the temperatures during the Cassini observations, but the greatest variations occur during day364, the first eclipse observation, which reaches the highest emission angle of all of the observations. The observed oscillations are greater than the $> 1\sigma$ uncertainties and are therefore considered to be real.

It is interesting that total intensity (Fig. 6) and temperature (Fig. 7) are not generally correlated. However, the final intensity data point for day364 is slightly elevated above previous points, and this corresponds to the highest temperature calculated during the eclipse observations. The total intensity data also revealed variation in Pele's emission over a longer timescale. If emission from Pele remained roughly constant throughout the three observations spanning four

days, then the data should all lie on the same curve in Fig. 6. It is clear, however, that separate curves must be drawn through the data for each eclipse, and that there is a gradual decrease in total emission from Pele from the first to the last eclipse observation (Fig. 6).

These are the first spacecraft observations of an Ionian eruption at this temporal resolution. With Galileo, observations of the same regions were repeated either minutes or months apart, but never several minutes apart over a two hour time period, and then again 40 hours later, and again 40 hours after that. We have now been able to document variability in thermal output at Pele on time scales of minutes, hours, days, months, and years. This volcano is remarkable in its constant behavior, especially given that hot lava erupts in spurts and cools rapidly.

2.2. Galileo I32 nightside observation

Galileo's final successful imaging flyby of Io, I32, occurred in October 2001 (Turtle et al., 2004). The I32 flyby provided us with five spectacular nightside images of Pele at 60 m pixel^{-1} . The images appear to have entirely covered the 30 km-wide patera and show some unexpected aspects of this unique volcano. Additionally, the Galileo NIMS instrument obtained observations of Pele in darkness at spatial resolutions of $\sim 1 \text{ km pixel}^{-1}$, allowing coanalysis of SSI and NIMS data (Davies et al., 2002).

2.2.1. Image details

The first three images were taken through the clear filter, which has a wavelength range of 380–1100 nm, and the second two images were taken through the $1 \mu\text{m}$ filter with a wavelength range of 950–1100 nm. Figure 8a is

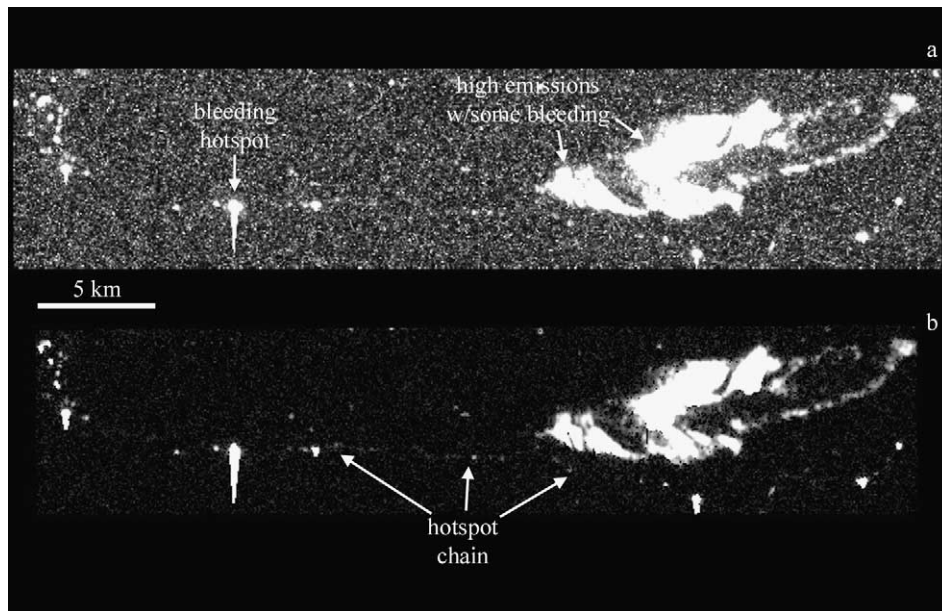


Fig. 8. Clear filter images of the Pele region from Galileo I32. (a) shows the raw data, illustrating the effect of radiation noise. (b) is the combination of the three clear images, using the noise removal technique described in Appendix A.2. A faint hotspot chain can be traced across the breadth of the "reduced noise" image.

a single, unprocessed, clear filter image of the Pele region. Several features are apparent in the raw image. Many of the bright spots in the image are saturated, and some are bleeding (as evidenced by the bright spikes pointing downward, see Appendix A.2 for more details). The bright central region also has some saturation and bleeding, and there are some interesting spatial patterns here. It is important to note that the images are extremely noisy, due to the charged-particle-laden environment in the vicinity of Jupiter. Thus, a noise removal technique was applied to the images (Appendix A.2). The reduced-noise images allow us to interpret the structures of the hot regions much more confidently. In particular, it is possible to trace a faint string of hotspots down from the upper left corner of the processed clear image (Fig. 8b), through the bright hotspots, below the bright central region, and back up the right side of the image. There is also an elongate bright ring of hotspots at the far right of the image. These strings of hotspots are similar to what was observed at slightly higher resolution in February 2000 (Fig. 3).

2.2.2. Temperatures of Pele from Galileo I32

We used the reduced-noise clear and infrared filter images to calculate color temperatures for the Pele region

(Appendix A.3). Since we had much better spatial resolution for these observations than for the Cassini observations, we could derive color temperatures across the hot lava within Pele Patera. Figure 9 is a close-up of a single-pixel-temperature image, in which each temperature has been assigned a color, ranging from dark red for lower temperatures, to bright yellow for higher temperatures, and white for saturation. Much of the middle region, near the large saturation areas, has color temperatures of about 1270 ± 100 K. There are also some hotter zones where pixels reach 1350 ± 200 , 1420 ± 300 , and 1605 ± 220 K. Some individual isolated pixels give exceedingly high color temperatures (up to 10,000 K), but also have correspondingly large errors. These are interpreted to be traces of radiation noise that we did not succeed in removing from the data (Appendix A.3). The temperature map shows that, as expected, most of the lower temperatures are at the outer margins of the high-emission areas, while the highest temperatures are closest to the saturated zones. In fact, it is likely that we are not measuring the highest color temperatures at Pele, since those are probably within saturated regions. This is possibly also the reason for the difference in temperature between the Cassini and Galileo observations. Regions of Pele that produced emission that saturated the Galileo cam-

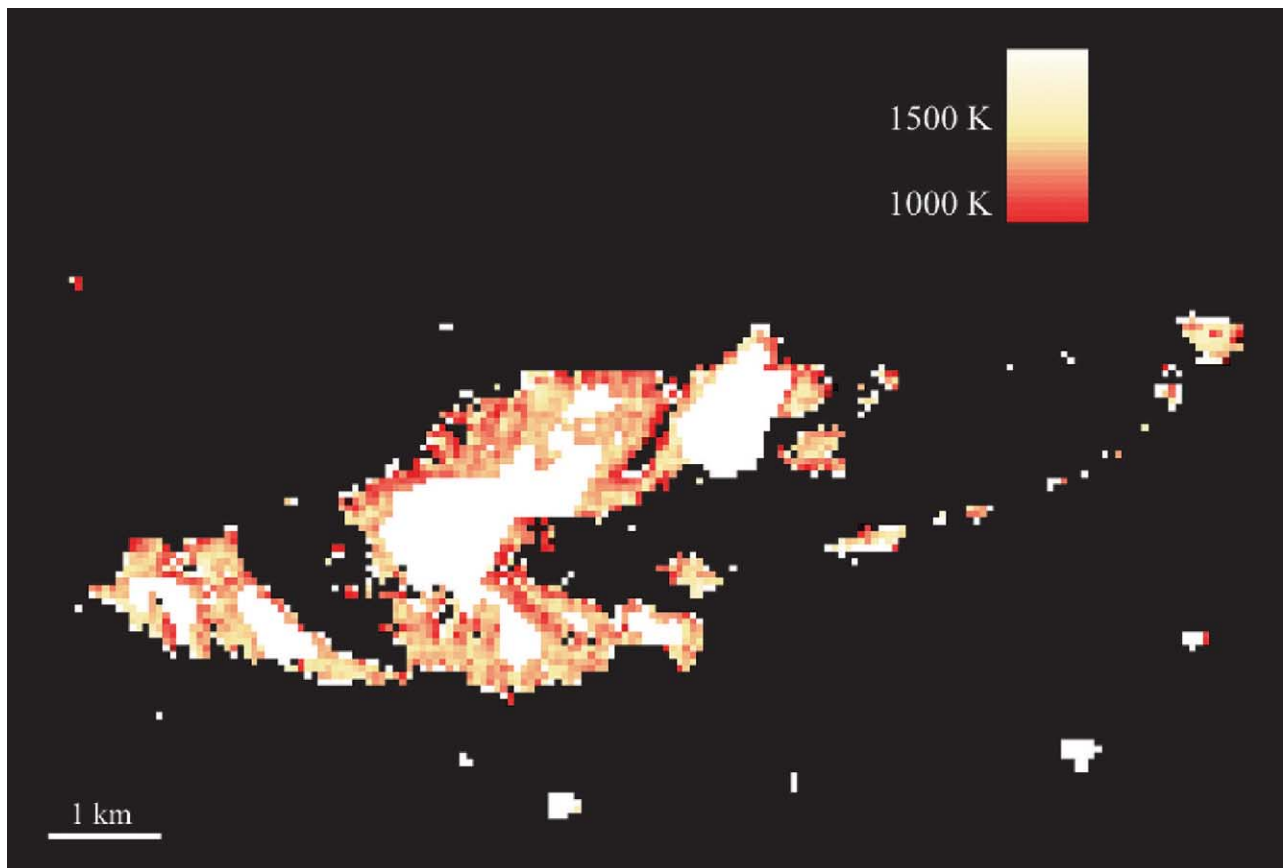


Fig. 9. Temperature map of the bright region of Pele Patera. In this image, the pixel values represent color temperatures according to the scale. White regions are areas of saturation and/or bleeding, for which temperatures could not be determined.

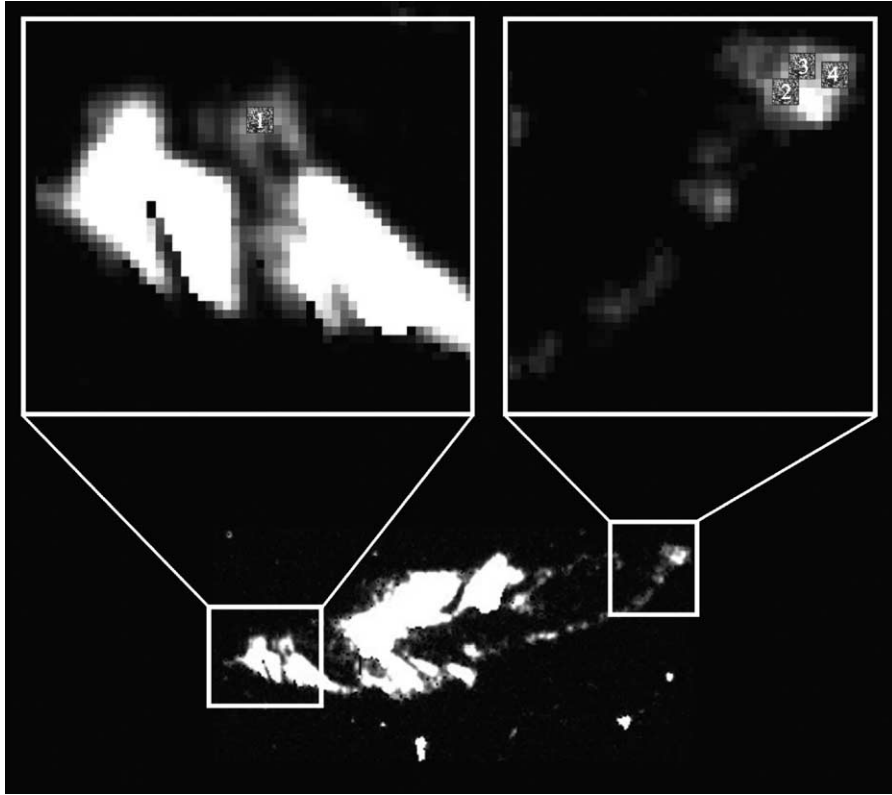


Fig. 10. Locations of four 3×3 pixel boxes selected from all possible 3×3 box combinations across the images for their high temperatures. Most of the high temperatures found are in the small hotspot in the upper right corner of Fig. 9.

era and could not be used for temperature calculations were included in our Cassini calculations of effective temperature.

A more precise estimate of the maximum color temperature can be found by using 3×3 box averages to further reduce the effect of radiation noise. Figure 10 shows where four boxes that were selected for their high temperatures are located on the reduced-noise clear image. Box 1, in the region just left of center, is 1294 ± 50 K. Boxes 2, 3, and 4 are all found in the large hotspot at the far right of the image. The color temperatures derived from using all the data in these boxes are, respectively, 1420 ± 100 , 1310 ± 60 , and 1390 ± 70 K. We note that these values are similar to those derived for the high-temperature components of two-temperature fits to NIMS data in Davies et al. (2001).

There is another way to look at these data that reveals something more about the nature of the Pele region. Figure 11 is a histogram of color temperatures from individual pixels. What is immediately apparent is that temperatures drop off rather steeply in both directions away from the modal value of 1270 K. There is a small range of temperatures for the majority of the Pele region, and then there are a few temperature values higher and lower than this. We fit the temperature distribution seen at Pele with two gaussian curves in an independent attempt to estimate the highest color temperatures that are likely to exist at Pele.

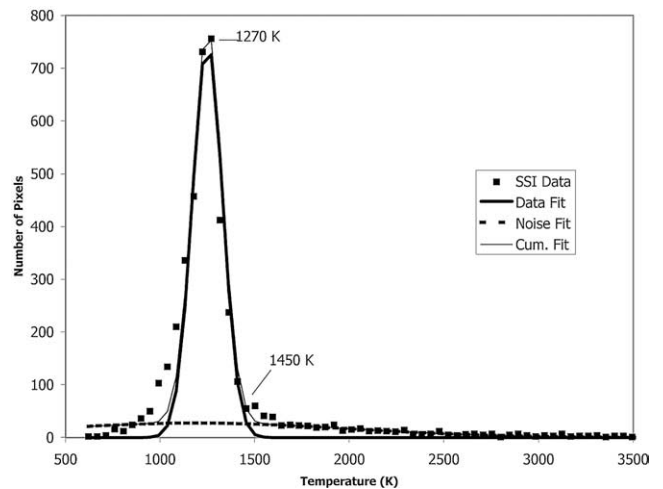


Fig. 11. Histogram of single pixel color temperatures. Two gaussian curves are shown; the first is a fit to the data that cluster around the mode of 1270 K, called “Data fit.” The second is a fit to undetectable (by SSI) or physically impossible temperatures, < 700 and > 2500 K.

The first curve was fit to what was assumed to be noise, i.e., the color temperatures > 2500 K. This fortuitously also provided a reasonable fit to the color temperatures < 700 K. These low temperatures must also be noise, because the SSI detector (at this exposure and gain setting) is not able to detect thermal emission from such cool surfaces. The remaining data were fit with another gaussian. This fit closely

matches the main peak in the histogram, suggesting that a large portion of Pele is close to 1270 K. The second gaussian also predicts that there should be a few valid pixels with color temperatures up to ~ 1500 K. It is intriguing that there is a small population of pixels between 1450 and 1600 K that are not fit with the two simple gaussians. This provides a hint that there may be a distinct population of smaller regions at these higher temperatures. However, we cannot prove that these higher temperatures are statistically meaningful.

3. Interpretation of recent Pele temperature data

3.1. Continuous energy output

The consistently high thermal output that was seen in all previous observations of Pele continued during both the Cassini and the Galileo I32 observations. Color temperatures of ~ 1350 K were seen throughout the 87 hour duration of the Cassini observations, and Galileo observed that > 5 km² of the Pele region were at about 1270 ± 100 K, with some smaller areas being even hotter. Rough estimates of the total thermal output of Pele, based on short-wavelength emission obtained during the Galileo I32 October 2001 observations, are consistent with the value of ~ 230 GW, calculated using NIMS data for orbits G2, G8, C10, E15, E16, and C20 (9/96–2/00) (Davies et al., 2001). Such long-lived, high thermal output is consistent with a persistent, high effusion rate eruption; however, there are no observed lavas erupting from the Pele region onto the nearby plains. This reinforces the conclusion reached by Davies et al. (2001) and Howell (1997) of a highly active, but confined, volcanic eruption: an active lava lake.

3.2. Temporal variability

The high temporal resolution of the Cassini observations of Pele enabled us to see variations in the eruption at visible and short infrared wavelengths over timescales of minutes (Fig. 7). This aspect of the eruption occurring at Pele has never been seen before on Io because of observational limitations, but it is typical of what happens at terrestrial lava lakes. From field observations of the Kupaianaha, Hawai'i, lava lake, Flynn et al. (1993) determined, from spectroradiometer data between 0.4 and 2.5 μm , that the thermal output from this lava lake varied on a time scale of seconds to minutes during phases of active overturning. The Cassini data of Pele show variation in activity on similar timescales at some of the same wavelengths; this observation suggests that a similar process to that at Kupaianaha may be taking place at Pele (albeit over a much larger area).

Flux density and temporal variation (or lack of variation) can also be used to constrain eruption style. The flux densities observed at Pele are very different than those from the ionian "Promethean" and "Pillanian" styles of eruption

(Keszthelyi et al., 2001). However, the flux and mass densities derived from NIMS E16 Pele data are very similar to those of the Kupaianaha lava lake during its most active phase, with fountaining and crustal disruption (Davies et al., 2001).

3.3. Decrease in emissions with rotation

Pele's rotation eastward during each eclipse reveals information about the morphology of the hot lava within the patera and its surrounding terrain. We found that the observed drop in intensity can be correlated with $[\cos(\text{emission angle})]^{1.6}$, significantly more pronounced than expected for a flat surface (Fig. 6). In fact, comparison with other data sets suggests that the variation in intensity with emission angle seems to be wavelength and therefore temperature dependent. Marchis et al. (2001) observed telescopically at 3.8 μm a decrease in energy from Pele with rotation of $[\cos(\text{emission angle})]^{1.3}$. From their observations, Marchis et al. (2001) concluded that there is topography, surrounding the patera or on its surface, that rotates into position to block some of the emitted light from reaching the camera, resulting in a greater decrease in intensity than would be seen for a flat source.

The best dayside images we have of Pele are from Voyager (Fig. 2), and they show that the patera is nestled in an east-west oriented graben, at the northern end of a large mountain (Danube Planum). This orientation of the major topographic features does not readily explain why thermal emission from Pele would be blocked as Pele rotated eastward with respect to Cassini. However, the high resolution Galileo SSI data suggest that a portion of the incandescent lava in Pele is located at the southwestern margin of the patera. These areas could be blocked if there is a near-vertical margin to Pele Patera, as was seen at Chaac and other paterae (e.g., Radebaugh et al., 2001). However, since these areas make up only a small fraction of the thermal emission seen at high resolution, this mechanism seems inadequate to explain the ISS observations.

We examine two other possibilities: cracks in the lava crust and lava fountains. Most cooling lava surfaces develop near-vertical cracks. When viewed from directly above, the hottest material at the base of the crack can be visible, but the effective temperature of the crack will rapidly diminish with increasing emission angle (Stansberry, 1999). If this were the dominant process at Pele, then the color temperatures should decrease dramatically with increasing emission angle. While we see a rapid decrease in total emissions with rotation (Fig. 6), we do not observe a decrease in temperature with rotation (Fig. 7). However, since cracks are essentially inevitable on any cooling lava surface, it is likely that some of the reduction in intensity as a function of emission angle should be attributed to cracks (Davies, 1996).

If Pele has a combination of a flat lava surface and lava fountains, then minor surrounding topography would preferentially block the low-lying lava surface. In this case,

as emission angle increases the color temperature would also increase because the thermal emission is progressively dominated by flux from the highly disrupted incandescent lava in the fountains. This effect could cancel the emission-decreasing effect of hot cracks. Furthermore, because lava fountains are typically very time-variable, we would expect the temperatures and thermal output to become significantly more erratic as emission angle increased. In addition, since the effect of incandescent fountains will be less pronounced on longer wavelength data (e.g., Keszthelyi and McEwen, 1997), this model predicts that Pele should more closely mimic a flat radiator at longer wavelengths, as observed. Thus the variation in color temperatures as a function of emission angle suggests that lava fountains contribute significantly to the thermal flux seen at Pele. Considering that a giant SO_2 plume is continually being erupted from the vicinity of Pele's incandescent region, we assume that as this gas exits the magma chamber, it disrupts the lava lake crust and creates fountains. The data are insufficient to determine if the fountains are more similar to terrestrial strombolian or hawaiian eruption styles. Based on active terrestrial lava lakes, strombolian-type activity is favored, but in Io's low gravity and near-vacuum, it is likely that the lava is thrown further than would be the case on Earth.

3.4. Details of the style of the Pele eruption

It was not possible to acquire high-resolution, dayside observations in conjunction with the Cassini and Galileo I32 observations; however, NIMS I32 data are sufficient to determine that there are no expanding warm areas that would correspond to lava flows extending from Pele (Fig. 12).

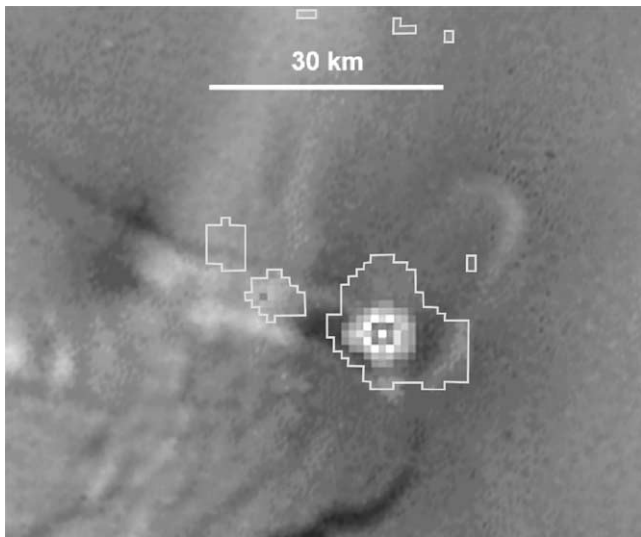


Fig. 12. NIMS observation of the Pele region, obtained at a range of ~ 4000 km during the I32 encounter on 16 October 2001, at ~ 1 km pixel $^{-1}$ resolution. Three distinct areas of thermal emission are seen, aligned along the rift at the end of Danube Planum. These areas coincide with the hottest areas seen in the SSI I32 image (see also Lopes et al., 2004; Davies et al., 2002). The positioning of the NIMS data on the Galileo SSI image is a best estimate.

Therefore, we conclude that the eruptions are confined to the patera, or to the large graben that contains the patera. A major eruption that is confined within a topographic depression will inevitably form a lava lake.

Burgi et al. (2002) studied the permanently active, 80 m diameter, basaltic lava lake at Erta Ale in Ethiopia in February 2001 (Fig. 13). While the entire Erta Ale lava lake would only be slightly larger than a single pixel in the I32 SSI Pele image, some valuable insights can be gained from the terrestrial analog. Burgi et al. (2002) observed that the lava lake exhibited three different states:

- (1) complete quiescence with no incandescent activity;
- (2) mild activity with some incandescent cracks; and
- (3) intense activity with incandescent cracks and fountaining.

The highest temperatures at Erta Ale were observed directly in the fountains, and the cracks and the crust were progressively cooler. Given the high temperatures seen at Pele over long timescales, we must be observing it always in the second or third state of activity, with incandescent cracks and/or fountaining, exposing the hot, young lava. The decrease in overall intensity from day364 to day001 in the Cassini observations (Fig. 6) could be due to fewer fountains or cracks in the Pele region exposing the hot material, a possible result of a decrease in input to the lava lake. The 200 K jump in temperature at the end of day364 could be due to a new pulse of fountaining.

Davies et al. (2001) calculated a mass flux into the circulating Pele lava lake system of $248\text{--}341$ m 3 s $^{-1}$. While this flux is orders of magnitude higher than mass fluxes at terrestrial lava lakes such as Erta Ale (up to 7 m 3 s $^{-1}$, see Harris et al., 1999), this estimate is very close to an earlier estimate by Carr (1986) of 350 m 3 s $^{-1}$, determined from Voyager IRIS data, under the assumption that thermal equilibrium had been reached between cooling lavas and the eruption of new material to maintain the observed thermal emission. The consistent volumetric flux between Voyager and Galileo observations is yet another demonstration of both the longevity and steadiness of volcanic activity at Pele.

The Galileo I32 October 2001 observation, although it was at night, gives us our most detailed picture of the distribution of activity inside the patera. The images do not reveal a large area of uniformly bright or hot material, rather there are three distinct regions within the patera that can be seen in Fig. 8. One is the vast, dark, background material that is emitting at temperatures too cool for the SSI camera to see (< 700 K) but which is easily seen in the NIMS high-resolution data (Fig. 12). We believe that this material is a cooled crust that has formed on top of parts of the lava lake (Fig. 13). Such a crust could be broken up by the second type of feature in the patera, the small, bright hotspots. These hotspots form a remarkably uniform, curving line that likely marks either the edge of the main patera or some secondary structural feature within the patera. We interpret



Fig. 13. Erta Ale lava lake, Ethiopia, in the Afar depression of the East African rift zone. Most of the $60 \text{ m} \times 100 \text{ m}$ active lava lake is shown in this image taken by Pierre Vetsch during a 1995 expedition. The lava lake crust is interrupted by cracks that separate the crust into plates, and by lava fountains, that occur both in the middle and where the crust breaks up at the margins.

these hotspots to be analogous to the disrupted incandescent margin that forms at the edge of the Erta Ale crater (Fig. 13) where the crust breaks up against the walls of the confining edifice, exposing the hot lava.

The third distinct feature of Pele Patera is the large, extremely bright, but patchy, central region. This region, and a couple of bright hotspots, can also be seen in the lower resolution, contemporaneous NIMS observation of the Pele region (Fig. 12; Davies et al., 2002). In the SSI data there are large regions (three or four separate areas of $\sim 2 \text{ km}^2$ each) of saturation and bleeding, for which we cannot obtain temperatures or see the detailed structure (Fig. 9). These are likely the locations of the most spatially extensive exposures of hot lava, exposed perhaps through convection and gaseous disruption of the cooling surface. The sources of the giant, 1500 km diameter plume deposit and the smaller, dark, pyroclastic apron are probably somewhere in this extremely active, central region, so there must be a continual flux of volatile-laden magma into this location. Therefore, the existence of the plume is consistent with large-scale fountaining, and possibly convection and overturn.

3.5. Eruption temperatures and composition

We observed color temperatures from 1300 ± 40 to $1500 \pm 80 \text{ K}$ during the eclipse observations of Pele by Cassini, and a median of 1270 K for single pixel values, or a maximum of $1420 \pm 100 \text{ K}$ from 3×3 pixel boxes, for the Galileo I32 observations. These numbers, especially those from the Cassini flyby, are fairly consistent with the temperatures that have been measured previously at Pele from other Galileo flybys and ground-based observations. They

are not, however, the highest temperatures measured at volcanoes on Io (McEwen et al., 1998a, 1998b; Davies et al., 2001). During the Galileo C9 flyby of Io in 1997, an outburst was observed at Pillan Patera, and temperatures were measured by SSI to be 1500–2600 K, and by a NIMS model to be 1825 K (McEwen et al., 1998b). Subsequent modeling of the combined NIMS-SSI dataset constrained minimum lava temperatures at Pillan to be $1870 \pm 25 \text{ K}$ (Davies et al., 2001).

The observed color temperatures are necessarily lower limits on the actual lava temperature. This is because in any pixel, there is a range of temperatures due to the formation of a chilled crust on the liquid lava. The wider this temperature range, the further the color temperature deviates from the eruption temperature of the liquid lava. At 61 km pixel^{-1} , the Cassini-derived temperatures could easily be hundreds of degrees lower than the actual eruption temperatures. Even at 60 m pixel^{-1} , the SSI single-pixel temperature estimates may be significantly below the actual eruption temperatures. However, if the activity at Pele were extremely vigorous, it would be plausible that regions thousands of square meters in area could be almost free of a chilled crust. Nonetheless, it is likely that the lavas at Pele are significantly hotter than 1400 K.

Precise lava compositions cannot be derived from lava temperatures. First, lavas are very rarely erupted at their liquidus temperatures; instead they are typically a lower temperature mixture of liquid, solid, and gas. It is even possible for lavas to be heated somewhat above their liquidus temperatures (e.g., Kargel et al., 2003; Keszthelyi et al., 2004). On the Earth, it is most typical for flowing lavas to be several

tens of degrees below their liquidus. Second, a given liquidus temperature does not uniquely define a lava composition.

Despite these caveats, there is a good relationship between lava temperature and broad categories of lava composition. Basalts most typically have liquidus temperatures of ~ 1300 – 1500 K. A basalt from Makaopuhi, Hawaii, with an iron- and magnesium-rich olivine and pyroxene and calcium-rich plagioclase mineralogy, ranges from a 1235 K solidus to a 1470 K liquidus, at the upper end of typical basaltic eruption temperatures (Wright and Okamura, 1977). The temperatures measured for the fountains of the basaltic Erta Ale lava lake were 1460 K (Burgi et al., 2002). In contrast, ancient terrestrial ultramafic komatiite lava flows were composed of a more mantle-like mineralogy of magnesium-rich olivine and pyroxene that reached liquidus temperatures of 1880 K (Williams et al., 2001). It is hypothesized that these lavas were generated by a high degree of partial melting of the mantle.

The derived temperatures presented in this analysis are towards the upper end of the basaltic range. However, given the limitations of deriving lava eruption temperature in the absence of in situ measurement, the possibility of ultramafic compositions at Pele cannot be ruled out.

4. Implications for Io's interior

At $30 \text{ km} \times 20 \text{ km}$, Pele is an extremely large volcano-tectonic depression by Earth's standards (Pike and Clow, 1981). Only the giant silicic calderas approach these dimensions, but they are not filled with mafic or ultramafic lava lakes. Thus Pele does not have a comparably sized terrestrial analog. Pele is similar to many other Ionian paterae in that they appear to also have been filled with lava during some stage of their evolution (Radebaugh et al., 2002; Lopes et al., 2004). Their great sizes indicate that a substantial volume of lava has been generated and delivered from Io's interior to its surface. However, Pele is a unique feature in its fountaining and constant expulsion of gas that is not typically seen at other paterae [an exception could be Tvashtar (Milazzo et al., in preparation)]. This demonstrates that Pele is an open system, that it is an active lava lake at the top of a magma column with a direct link to a recirculating subsurface magma supply (see Section 1). Other paterae may currently be inactive lava lakes or just be filled with ponded lavas. These are analyzed differently since the resulting mass and energy fluxes are determined by topography (which we do not know) more than mechanism of supply (Davies, 2003).

Volatiles set Pele apart from other ionian volcanic centers by forming the plume, fueling the lava fountains, expelling the silicate magmas to be deposited in the dark pyroclastic deposit surrounding the patera, and being ejected to form the giant short-chain sulfur ring surrounding Pele. Thermodynamic calculations of the composition of Pele's plume in

equilibrium with a 1440 K magma match observations of the gas species ratios (Zolotov and Fegley, 2000; Spencer et al., 2000b). Thus, the majority of Pele's plume gases should be dissolved in the magma at depth, to be exsolved at low pressures upon eruption, rather than being released from nearby crustal reservoirs of sulfur heated by silicate magma. Davies et al. (2001) determined that the lack of lava flows surrounding Pele, and strong localization of volcanic activity, means that the short-chain sulfur molecules in the plume are exsolving from the erupting magma, and do not result from mobilization of sulfur compounds on the surface in the manner of the Prometheus plume (Kieffer et al., 2000; Milazzo et al., 2001). Given the high rate of volcanic activity over geologic time, it is expected that Io's interior is depleted in volatiles. If Io lost its internal volatiles through volcanic activity, then currently there must be a mechanism by which volatiles are recycled into the magma. Perhaps this occurs by extremely rapid burial of volatile-enriched crustal materials that are subsequently supplied to ascending magma columns.

The lack of impact craters and high rate of volcanic activity on Io's surface attest to Io's very high resurfacing rate (Johnson and Soderblom, 1982; Phillips, 2000). This leads to subsidence in the crust (O'Reilly and Davies, 1981; Carr et al., 1998; Schenk and Bulmer, 1998; Turtle et al., 2001; Jaeger et al., 2003), which carries volatiles to great depths before they become liquid (Keszthelyi et al., 2004). Crustal subsidence also generates regional compressive stresses, driving mountain formation (Schenk and Bulmer, 1998; Turtle et al., 2001; Jaeger et al., 2003). Once these compressive stresses are relieved, the crustal faults associated with mountain building can be exploited by magmas ascending to the surface (Turtle et al., 2001; Jaeger et al., 2003). This process may lead to the formation of large, shallow sills, and subsequent mobilization of overlying, volatile-rich material would then lead to patera formation (Keszthelyi et al., 2004). Mountains and paterae are tectonically, and perhaps genetically, linked, as more than 40% of all mountains are associated with paterae (Jaeger et al., 2003). Even Pele Patera is adjacent to Danube Planum, so perhaps Pele's magmas ascended along crustal fractures associated with Danube's creation (Fig. 14).

This recent work adds to our study of paterae on Io (Radebaugh et al., 2001), and furthers the understanding of these large, long-lived, volcano-tectonic depressions as significant features for the release of heat from Io's interior. There is a strong dichotomy between these extremely hot, active paterae that cover only about 2.5% of the surface of Io (Zhang et al., 2002) and the cold, surrounding crust. The implications of our results provide confirmation of earlier indications (e.g., McEwen et al., 1985) that the tremendous heat flow through Io's lithosphere is extremely spatially discrete.

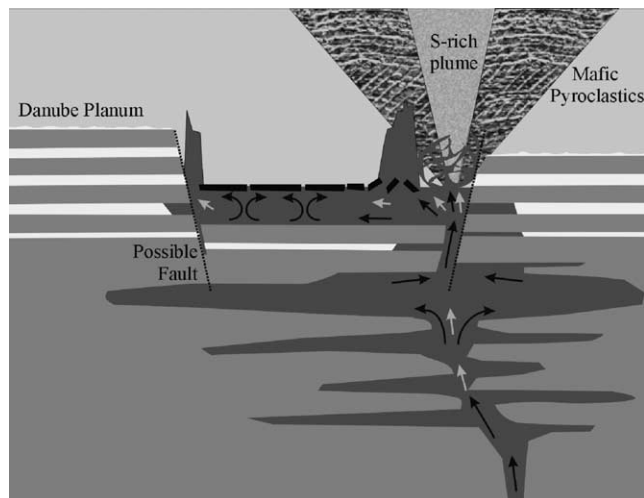


Fig. 14. Hypothetical cross section of the lava lake at Pele Patera. Silicate layers are interspersed with SO_2 deposits (see Carr et al., 1979). It has been shown by Johnson et al. (1995) that these deposits can be trapped between lava flows and buried, without being entirely driven off. Magma rises through fractures in the crust, possibly along old fault zones related to the formation of Danube Planum (Turtle et al., 2001; McKinnon et al., 2001), to form a high-level magma chamber. Volatiles rise with the magma and exsolve at the surface through bubble bursts and lava fountains, and create the giant plume and mafic pyroclastic eruptions. Aspects of the drawing are not to scale.

5. Conclusions

Two exceptional data sets were analyzed to obtain information about the eruption style and temperature of the Pele volcano on Io. We found color temperatures for Pele as high as 1500 ± 80 K from Cassini and 1605 ± 220 K or 1420 ± 100 K from Galileo I32. Actual lava temperatures could be hundreds of degrees higher, so compositions ranging from basaltic to ultramafic should be considered for Pele's lavas. The high temperatures, their variation over all timescales, and the decrease in brightness with rotation by a factor of $[\cos(\text{emission angle})]^{1.6}$, along with Pele's consistent activity as evidenced by the continually replenished giant ring of volatiles, lend further credence to the model of Pele as a vigorously active, fountaining lava lake.

Acknowledgments

The authors express their thanks to Paul Geissler for his help with Cassini image processing. This material is based upon work supported by the National Aeronautics and Space Administration under Grant Nos. NAG5-10166 and NAGW5-3632 issued through the Planetary Geology and Geophysics Program, and by the Cassini project. Ashley Davies is supported by Grant No. 344-30-23-09 through the NASA Planetary Geology and Geophysics program. All images were processed at PIRL, the Planetary Image Research Laboratory, unless otherwise stated.

Appendix A

A.1. Modeling Cassini color temperatures from two-filter ratios

Here we detail how we computed color temperatures from the multi-filter Cassini ISS data. We use color temperature because it generally provides a better temperature estimate than brightness temperature (which is derived from single filter images). Color temperature is derived from the variations of blackbody thermal radiation (i.e., the Planck function) as a function of wavelength. As such, only the relative intensities at different wavelengths need to be measured; therefore, many wavelength independent factors needed to calculate absolute radiances can be safely ignored.

ISS has two filter wheels in front of each camera, so that all observations are taken through two filters. Commonly a clear filter (CL1 or CL2) is selected in one filter wheel while a filter with a narrower bandpass is selected for the other wheel. Selecting clear filters in both wheels (CL1 and CL2) allows maximum light transmission (Porco et al., 2003). The Pele data have the best signal-to-noise ratio in the clear filter pair (CL1–CL2, transmitting 200–1050 nm), and the infrared filter pair (IR4–CL2, transmitting 875–1050 nm), so images obtained through these filters were used together to obtain color temperatures. To determine the response of the ISS camera through each filter, we integrated, across the range of wavelengths to which the detector is sensitive, the product of

- blackbody thermal radiation at specific temperatures,
- the ISS detector's wavelength-dependent response, and
- the filter transmissivity.

This was only possible because the camera and filter responses were measured to $\sim 1\%$ absolute accuracy at every 10 nm of wavelength. These pre-flight calibrations have been repeatedly tested in-flight, providing us with the highest possible level of radiometric precision. Camera responses were calculated for blackbody temperatures from 600 to 2500 K, at 100 K intervals. A constant emissivity of 1 was used in our calculations, but the value for emissivity cancels when the signal from two filters is ratioed during the calculation of color temperatures. Since there are no known strong spectral features in this part of the lava's emission spectrum, this seems a reasonable assumption. Ratios of integrated blackbody radiation in the clear and the infrared wavelength ranges are plotted against the corresponding blackbody temperatures (Fig. A.1). This plot is compared with ratios of actual emission from Pele observed through the CL1–CL2 and IR4–CL2 filter pairs through interpolation to determine color temperature.

The image resolution is $\sim 61 \text{ km pixel}^{-1}$ for all of these observations, so the Pele hotspot is much smaller than one pixel. However, the hotspot appears similar to stars in the same image, in that the emission from Pele is distributed

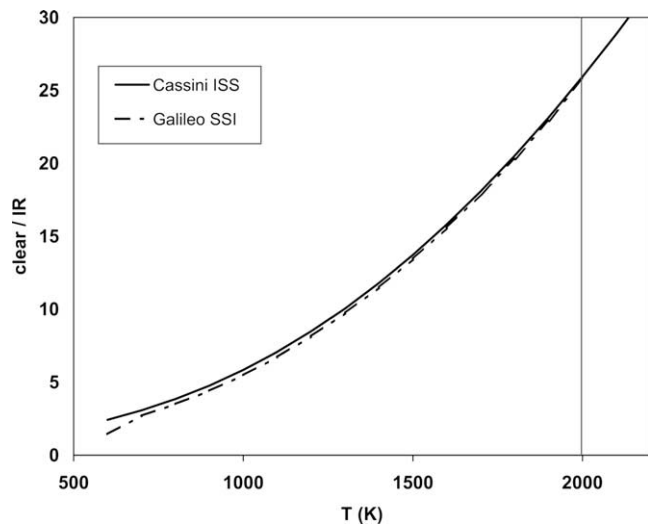


Fig. A.1. Ratios of expected blackbody emission through the clear and IR filters for the Cassini ISS (solid line) and Galileo SSI (dashed line) cameras. Notice how similar the responses are for the two cameras, especially at high temperatures.

across a 9×9 pixel box due to the ISS point spread function. To determine the total output from Pele in terms of DN s^{-1} , where DN = data number corresponding to the camera's response to scene intensity, we measured the mean DN values for the 9×9 pixel areas containing the Pele hotspot in the clear and infrared images. To remove the contribution to the signal from background radiation, we obtained mean DN background radiation values for two 9×9 pixel boxes, one on Io's disk near the Pele hotspot but away from auroral glows and other hotspots, and the other in deep space, away from Io's disk. The average of the two background DN values was subtracted from the mean DN value for the hotspot.

The overall "signal" for Pele, in DN s^{-1} , is given by the relationship:

$$\text{signal} = (\text{DN}_{\text{mean}} - \text{DN}_{\text{bg}})n/t, \quad (1)$$

where DN_{mean} is the mean DN value of the 9×9 box containing Pele, DN_{bg} is the mean background value in DN, n is number of pixels in the "sample" ($9^2 = 81$, in this case), and t is the exposure time in seconds (2 s for all images, except the infrared images in day000, which were 3.2 s). We then divided the clear signal by the infrared signal to determine the ratio, which we converted to temperature by interpolating between the ratio values that were calculated at 100 K intervals, as described earlier. The results are plotted in Fig. 5.

Uncertainties in the temperatures are dominated by background noise. Therefore, we found the standard deviation (σ) for data in each of the Cassini images by finding σ of the mean background values. This σ was then used to find the standard error (SE), which is a measurement of the typical size of the chance variation of the "sample" value (Stark, 1997). The SE is dependent on the size of the sample, which for our measurements of the average DN of the Pele hotspot

was 81 pixels. The SE was found using the following relationship:

$$\text{SE} = \sigma/n^{1/2}, \quad (2)$$

where n is the number of pixels in a sample. This error was applied to the ratios by the same procedure used by McEwen et al. (1998b): adding the SE on the clear filter image to the clear filter DN value, subtracting the infrared filter SE from the infrared filter DN value, then taking the ratio of these results to obtain the maximum value within the error bars for a given ratio. Replacing "adding" with "subtracting" in each case resulted in obtaining the minimum ratio value. This method provides $> 1\sigma$ limits, so we have reasonable confidence that our results are within our stated uncertainties. These maximum and minimum ratio values have been converted to the error bars in Fig. 5.

A.2. Galileo I32 image details and noise-reduction technique

Each of the 3 clear and 2 infrared Galileo images was separated by only ~ 9 seconds, and the exposure times were 0.046 seconds for the clear and 0.196 seconds for the $1 \mu\text{m}$ images. Despite these short exposure times, in every image some pixels were saturated and even bleeding, because of the intense emissions from small portions of Pele. When pixels in the CCD of the camera become over-filled, they bleed electrons to other pixels along the same column at a ratio of 1 electron to the pixel above to 10 electrons to the pixel below. Figure 8a shows that many of the bright spots in the unprocessed clear filter image have dramatic downward spikes caused by bleeding, for example the large spike left of center is probably a hotspot just 10 or 12 pixels in diameter. The large bright region of high emission right of center also has locations with bleeding. This effect has been seen before at Io in other instances of intense thermal emission, for example, the eruption at Tvashtar Catena (Keszthelyi et al., 2001). In fact, this process is sufficiently well quantified that it has been used to derive accurate estimates of the intensity of the thermal emission (e.g., McEwen et al., 1998b).

It is important to note that the image is extremely noisy. The high-energy particles close to Jupiter affect the SSI camera in two ways. The highest energy "hits" cause distinct bright spots or streaks, while the more numerous lower energy particles raise the background DN level. To decrease the noise and allow for better analysis of the data, we used the fact that we have multiple images through the same filter to identify and remove radiation "hits" using the following algorithm. First, the three clear filter images were co-registered so each pixel in each image corresponded to the same location on the surface. Then, if a pixel in clear image A was within $\pm 50\%$ of the value of the same pixel in clear images B and C, the mean value from images A, B, and C was placed in a new image. Otherwise, the pixel was given a null value in the new image. The resulting image has most of the obvious radiation hits removed (Fig. 8b).

The same technique was also applied to the two 1 μm images.

A.3. Galileo I32 two-filter color temperature derivation and error analysis

The reduced-noise clear and 1 μm images were used to determine temperatures of the bright regions at Pele Patera. The same method discussed in Appendix A.1 for finding 2-filter color temperatures from Cassini ISS images was also applied to these Galileo SSI images, with minimal variation. We used information about the SSI camera response to blackbody radiation through the clear and 1 μm filters to create a graph of the ratio of clear to 1 μm emissions vs. temperature (McEwen et al., 1997; Klaasen et al., 1997). This function is plotted in Fig. A.1 alongside that for Cassini.

However, since we wanted to take advantage of the high spatial resolution of the Galileo data, we did not average the emissions over many-pixel portions of the image. Instead, we derived ratios (and thus color temperatures) for individual pixels, avoiding regions of saturation and bleeding. In addition, all pixels with a signal < 20 DN were eliminated from the images because the signal-to-noise ratio in those pixels was insufficient to allow accurate temperature estimates. Each pixel in the reduced-noise clear image was ratioed with the corresponding pixel in the reduced-noise 1 μm image. Where valid data were available in both images, the resulting ratio was converted to a temperature using the following fit to the curve in Fig. A.1:

$$T = 608.096 + 304[\ln(0.5202 \times R)]^{1.595}. \quad (3)$$

Again, the uncertainty in our measurements was dominated by background noise. Therefore, we found the standard deviation (σ) for the data in each of the raw Galileo images by finding σ of the mean of an 81×81 pixel background box, away from the region of high emission. We selected a large box to increase the accuracy of the determination of σ .

This σ was then used to find the standard error (SE), Eq. (2). The SE is dependent on the size of the sample, which for our measurements were $1 \times 1 = 1$ pixel boxes. However, estimating temperatures for single pixels leads to large uncertainties. Therefore, in addition to 1×1 pixel ratios, we selected 3×3 pixel regions that appeared to have especially high emission (and no saturation) to obtain more precise temperature estimates. Pixel boxes of size 3×3 were chosen because they were small enough to contain high-temperature material, but large enough to significantly reduce the uncertainties. Note that for a sample size of 1 pixel, Eq. (2) reduces to

$$SE = \sigma, \quad (4)$$

which mathematically demonstrates why the uncertainty on the temperatures found for a single pixel is relatively large.

References

- Burgi, P., Caillet, M., Haefeli, S., 2002. Field temperature measurements at Erta'Ale lava lake, Ethiopia. *Bull. Volcanol.* 64 (7), 472–485. 10.1007/s00445-002-0224-3.
- Carr, M.H., Masursky, H., Strom, R.G., Terri, R.J., 1979. Volcanic features of Io. *Nature* 280, 729–733.
- Carr, M.H., 1986. Silicate volcanism on Io. *J. Geophys. Res.* 91, 3521–3532.
- Carr, M.H., McEwen, A.S., Howard, K.A., Chuang, F.C., Thomas, P., Schuster, P., Oberst, J., Neukum, G., Schubert, G., 1998. Mountains and calderas on Io: possible implications for lithosphere structure and magma generation. *Icarus* 135, 146–165.
- Davies, A.G., 1996. Io's volcanism: thermo-physical models of silicate lava compared with observations of thermal emission. *Icarus* 124, 45–61.
- Davies, A.G., 2003. Temperature, age and crust thickness distributions of Loki Patera on Io from Galileo NIMS data: implications for resurfacing mechanism. *Geophys. Res. Lett.* In press.
- Davies, A.G., Keszthelyi, L.P., Williams, D.A., Phillips, C.B., McEwen, A.S., Lopes, R.M.C., Smythe, W.D., Kamp, L.W., Soderblom, L.A., Carlson, R.W., 2001. Thermal signature, eruption style, and eruption evolution at Pele and Pillan on Io. *J. Geophys. Res.* 106, 33079–33104.
- Davies, A.G., 14 colleagues, 2002. The lava lake at Pele: an analysis of high-resolution, multi-wavelength Galileo data. In: *Proc. Lunar Planet. Sci. Conf. 33rd. Abstract 1162 [CD-ROM]*.
- Flynn, L.P., Mougini-Mark, P.J., Gradie, J.C., Lucey, P.G., 1993. Radiative temperature measurements at Kupaianaha lava lake, Kilauea volcano, Hawaii. *J. Geophys. Res.* 98, 6461–6476.
- Geissler, P.E., McEwen, A.S., Keszthelyi, L., Lopes-Gautier, R., Granahan, J., Simonelli, D.P., 1999. Global color variations on Io. *Icarus* 140, 265–282.
- Harris, A.J.L., Flynn, L.P., Rothery, D.A., Oppenheimer, C., Sherman, S.B., 1999. Mass flux measurements at active lava lakes: implications for magma recycling. *J. Geophys. Res.* 104, 7117–7136.
- Howell, R.R., 1997. Thermal emission from lava flows on Io. *Icarus* 127, 394–407.
- Jaeger, W.L., Turtle, E.P., Keszthelyi, L.P., Radebaugh, J., McEwen, A.S., Pappalardo, R.T., 2003. Orogenic tectonism on Io. *J. Geophys. Res.* 108 (E8), 5094. 10.1029/2002JE001946.
- Johnson, T.V., Soderblom, L.A., 1982. Volcanic eruptions on Io: implications for surface evolution and mass loss. In: Morrison, D. (Ed.), *Satellites of Jupiter*. Univ. of Arizona Press, Tucson, pp. 634–646.
- Johnson, T.V., Matson, D.L., Blaney, D.L., Veeder, G.J., Davies, A.G., 1995. Stealth plumes on Io. *Geophys. Res. Lett.* 22, 3293–3296.
- Kargel, J.S., Carlson, R.W., Davies, A.G., Fegley Jr., B., Gillespie, A., Greeley, R., Howell, R.R., Jessup, K.L., Kamp, L., Keszthelyi, L.P., Lopes, R.M., MacIntyre, T.J., Marchis, F., McEwen, A.S., Milazzo, M., Perry, J., Radebaugh, J., Schaefer, L., Schmer, N., Smythe, W.D., Spencer, J.R., Williams, D.A., Zhang, J., Zolotov, M., 2003. Extreme volcanism on Io: latest insights at the end of the Galileo era. *EOS Trans. AGU* 84, 313.
- Keszthelyi, L., McEwen, A., 1997. Magmatic differentiation of Io. *Icarus* 130, 437–448.
- Keszthelyi, L., 12 colleagues, 2001. Imaging of volcanic activity on Jupiter's moon Io by Galileo during the Galileo Europa Mission and the Galileo Millennium Mission. *J. Geophys. Res.* 106, 33025–33052.
- Keszthelyi, L., Jaeger, W.L., Turtle, E.P., Milazzo, M., Radebaugh, J., 2004. A post-Galileo view of Io's interior. *Icarus* 169, 271–286.
- Kieffer, S.W., Lopes-Gautier, R., McEwen, A., Smythe, W., Keszthelyi, L., Carlson, R., 2000. Prometheus: Io's wandering plume. *Science* 288, 1204–1208.
- Klaasen, K.P., Belton, M.J.S., Breneman, H.H., McEwen, A.S., Davies, M.E., Sullivan, R.J., Chapman, C.R., Neukum, G., Heffernan, C.M., 1997. Inflight performance characteristics, calibration, and utilization of the Galileo solid-state imaging camera. *Opt. Eng.* 36, 3001–3027.
- Lopes-Gautier, R., 11 colleagues, 1999. Active volcanism on Io: global distribution and variations in activity. *Icarus* 140, 243–264.

- Lopes, R.M.C., 14 colleagues, 2001. Io in the near infrared: Near-Infrared Mapping Spectrometer (NIMS) results from the Galileo flybys in 1999 and 2000. *J. Geophys. Res.* 106, 33053–33078.
- Lopes, R.M.C., Kamp, L.W., Smythe, W.D., Mougins-Mark, P., Kargel, J., Radebaugh, J., Turtle, E.P., Perry, J., Williams, D., Carlson, R.W., Douté, S., 2004. Lava lakes on Io: observations of Io's volcanic activity from Galileo NIMS during the 2001 flybys. *Icarus* 169, 140–174.
- Marchis, F., Prange, R., Fusco, T., 2001. A survey of Io's volcanism by adaptive optics observations in the 3.8- μ m thermal band (1996–1999). *J. Geophys. Res.* 106, 33141–33159.
- McEwen, A.S., Matson, D.L., Johnson, T.V., Soderblom, L.A., 1985. Volcanic hot spots on Io: correlation with low-albedo calderas. *J. Geophys. Res.* 90, 12345–12379.
- McEwen, A.S., Simonelli, D.P., Senske, D.R., Klaasen, K.P., Keszthelyi, L., Johnson, T.V., Geissler, P.E., Carr, M.H., Belton, M.J.S., 1997. High-temperature hot spots on Io as seen by the Galileo Solid State Imaging (SSI) experiment. *Geophys. Res. Lett.* 24, 2443–2446.
- McEwen, A.S., 13 colleagues, 1998a. Active volcanism on Io as seen by Galileo SSI. *Icarus* 135, 181–219.
- McEwen, A.S., 14 colleagues, 1998b. High-temperature silicate volcanism on Jupiter's moon Io. *Science* 281, 87–90.
- McEwen, A.S., 25 colleagues, 2000. Galileo at Io: results from high-resolution imaging. *Icarus* 288, 1193–1198.
- McKinnon, W.B., Schenk, P.M., Dombard, A.J., 2001. Chaos on Io: a model for formation of mountain blocks by crustal heating, melting, and tilting. *Geology* 29, 103–106.
- Milazzo, M.P., Keszthelyi, L.P., McEwen, A.S., 2001. Observations and initial modeling of lava-SO₂ interactions at Prometheus, Io. *J. Geophys. Res.* 106, 33121–33127.
- Miner, E.D., 2002. The Cassini-Huygens Mission to Saturn and Titan. Astronomical Data Analysis Software and Systems XI. In: Bohlender, D.A., Durand, D., Handley, T.H. (Eds.), ASP Conf. Proc., vol. 281. Astronomical Society of the Pacific, San Francisco, p. 373.
- O'Reilly, T.C., Davies, G.F., 1981. Magma transport of heat on Io: a mechanism allowing a thick lithosphere. *Geophys. Res. Lett.* 8, 313–316.
- Pearl, J.C., Sinton, W.M., 1982. Hot spots of Io. In: Morrison, D. (Ed.), *Satellites of Jupiter*. Univ. of Arizona Press, Tucson, pp. 724–755.
- Phillips, C.B. 2000. *Voyager and Galileo views of Volcanic resurfacing on Io and the search for geologic activity on Europa*. PhD thesis, Univ. of Arizona, Tucson, 269 p.
- Pike, R.J., Clow, G.D., 1981. Revised classification of terrestrial volcanoes and catalog of topographic dimensions, with new results on edifice volume. US Geol. Survey Open File Report 81-1038, 40 p.
- Porco, C.C., 23 colleagues, 2003. Cassini imaging of Jupiter's atmosphere, satellites, and rings. *Science* 299, 1541–1547.
- Radebaugh, J., 1999. *Terrestrial Pluton and planetary caldera sizes: implications for the origin of calderas*. MS thesis. Brigham Young Univ., Provo, Utah.
- Radebaugh, J., McEwen, A., 2001. Temperatures of Io's Pele hotspot from Cassini eclipse images. In: AAS DPS Meeting 33rd. Abstract 563.
- Radebaugh, J., Keszthelyi, L., McEwen, A., Turtle, E., Milazzo, M., Jaeger, W., 2001. Paterae on Io: a new type of volcanic caldera? *J. Geophys. Res.* 106, 33005–33020.
- Radebaugh, J., McEwen, A.S., Milazzo, M., Davies, A.G., Keszthelyi, L.P., Geissler, P., Turtle, E.P., 2002. Lava Lakes in Io's Paterae. *EOS Trans. AGU Spring Meet. Suppl.* 83 (19), 33005–33020. Abstract P21B-06.
- Rathbun, J.A., Spencer, J.R., Tamppari, L.K., Martin, T.Z., Barnard, L., Travis, L.D., 2004. Mapping of Io's thermal radiation by the Galileo Photopolarimeter–Radiometer (PPR) instrument. *Icarus* 169, 127–139.
- Schenk, P.M., Bulmer, M.H., 1998. Origins of mountains on Io by thrusting, faulting and large-scale mass movements. *Science* 279, 1514–1517.
- Smith, B.A., The Voyager Imaging Team, 1979. The Jupiter system through the eyes of Voyager 1. *Science* 204, 951–971.
- Spencer, J.R., Schneider, N.M., 1996. Io on the eve of the Galileo mission. *Annu. Rev. Earth Planet Sci.* 24, 125–190.
- Spencer, J.R., Sartoretti, P., Ballester, G.E., McEwen, A.S., Clarke, J.T., McGrath, M.A., 1997a. The Pele plume (Io); observations with the Hubble Space Telescope. *Geophys. Res. Lett.* 24, 2471–2474.
- Spencer, J.R., McEwen, A.S., McGrath, M.A., Sartoretti, P., Nash, D.B., Noll, K.S., Gilmore, D., 1997b. Volcanic resurfacing of Io: post-repair HST imaging. *Icarus* 127, 221–237.
- Spencer, J.R., Jessup, K.L., McGrath, M.A., Ballester, G.E., Yelle, R., 2000a. Discovery of gaseous S₂ in Io's Pele plume. *Science* 288, 1208–1210.
- Spencer, J.R., Rathbun, J.A., Travis, L.D., Tamppari, L.K., Barnard, L., Martin, T.Z., McEwen, A.S., 2000b. Io's Thermal Emission from the Galileo Photopolarimeter–Radiometer. *Science* 288, 1198–1201.
- Stansberry, J.A., 1999. Thermal emission from Io's lava flows; spectral dependence on emission angle. In: *Proc. Lunar Planet. Sci. Conf. 30th. Abstract 2009*.
- Stark, P.B., 1997. Stici Gui: statistics tools for internet and classroom instruction with a graphical user interface. Online publication, <http://www.stat.Berkeley.EDU/users/stark/SticiGui/index.htm>.
- Strom, R.G., Terriale, R.J., Masursky, H., Hansen, C., 1979. Volcanic eruption plumes on Io. *Nature* 280, 733–736.
- Strom, R.G., Schneider, N.M., Terriale, R.J., Cook, A.F., Hansen, C.J., 1981. Volcanic eruptions on Io. *J. Geophys. Res.* 86, 8593–8620.
- Turtle, E.P., Jaeger, W.L., Keszthelyi, L.P., McEwen, A.S., Milazzo, M., Moore, J., Phillips, C.B., Radebaugh, J., Simonelli, D., Chuang, F., Schuster, P., 2001. Mountains on Io: high-resolution Galileo observations, initial interpretations, and formation models. *J. Geophys. Res.* 106, 33173–33200.
- Turtle, E.P., 14 colleagues, 2004. The final Galileo SSI observations of Io: orbits G28–I33. *Icarus* 169, 3–28.
- Williams, D.A., Greeley, R., Lopes-Gautier, R., Davies, A., 2001. Evaluation of sulfur flow emplacement on Io from Galileo data and numerical modeling. *J. Geophys. Res.* 106, 33105–33119.
- Wright, T.L., Okamura, R.T., 1977. Cooling and crystallization of tholeiitic basalt: Makaopuhi lava lake, Hawaii. US Geol. Survey Prof. Paper 1004.
- Zhang, Q., Radebaugh, J., Turtle, E.P., Keszthelyi, L.P., Milazzo, M.P., Jaeger, W.L., McEwen, A.S., 2002. Investigation of the distribution and characteristics of ionian paterae using a relational database. In: *Proc. Lunar Planet. Sci. Conf. 33rd. Abstract 1745 [CD-ROM]*.
- Zolotov, M.Y., Fegley, B., 2000. Eruption conditions of Pele volcano on Io inferred from chemistry of its volcanic plume. *Geophys. Res. Lett.* 27, 2789–2792.